Self-consistent calculations of charge self-trapping energies: A comparative study of polaron formation and migration in $PbTiO_3$

Elaheh Ghorbani,[1,*] Lorenzo Villa,[1] Paul Erhart,[2] Andreas Klein,[3] and Karsten Albe[1]

[1]*Fachgebiet Materialmodellierung, Institut für Materialwissenschaft, TU Darmstadt, Otto-Berndt-Straße 3, D-64287 Darmstadt, Germany*

[2]*Department of Physics, Chalmers University of Technology, SE-412 96 Gothenburg, Sweden*

[3]*Fachgebiet Elektronische Struktur von Materialien, Institut für Materialwissenschaft, TU Darmstadt, Otto-Berndt-Straße 3, D-64287 Darmstadt, Germany*

(Received 23 July 2021; revised 19 May 2022; accepted 21 June 2022; published 28 July 2022)

This study presents a systematic assessment of the behavior of self-trapped electrons in $PbTiO_3$, which is a prototypical ferroelectric material with a wide range of technological applications. Since modeling of polarons depends sensitively on the applied method, the goal of this work is to identify the parameters used in density functional theory (DFT), which allow to predict the properties of polarons with high accuracy. The DFT+U method is employed to benchmark how the choice of k-mesh grids, lattice parameters, and pseudopotential (PP) affects the polaron trapping energy. Then, the appropriate parameters were used to study polaron trapping energy and its optical transition using the HSE06 hybrid functional. It is shown that the magnitude of the trapping energy is highly sensitive to the choice of the PP and the applied lattice parameters. A comparison of polaron trapping energies using the two functionals indicates proximity of the DFT+U result to the HSE06 result. Finally, configuration coordinate diagrams for the polaron-associated absorption and luminescence peaks in $PbTiO_3$ are presented and compared to experiments.

DOI: 10.1103/PhysRevMaterials.6.074410

I. INTRODUCTION

The dissociation of short-lived excitons gives rise to free electrons and holes. If coupled with the motion of nuclei, these free charges get trapped at a lattice site and polarons form. Due to the involvement of lattice distortions in the formation of polarons, their lifetime exceeds that of excitons. The prediction of polaronic states is therefore important for understanding the structural, electronic, magnetic, and optical properties of materials. Electron (hole) polarons with large migration barriers, for example, impede n-type (p-type) conductivity of the material [1], while those with low activation barriers trigger electrical conductivity [2,3]. Polarons can also affect electronic properties of optoelectronic devices by stimulating and/or impeding the recombination of photogenerated electrons and holes [4,5]. In addition, the existence of polarons can alter the optical properties of the host material, manifesting itself in specific absorption and/or emission bands [6–12]. Polaron formation also plays a role in charge compensation mechanisms and can cause Fermi level pinning [13–15]. A quantitative determination of the carrier (self-)trapping energy and its electronic energy level is thus essential for designing materials with respect to a specific application.

Experimentally, valuable information on polarons can be obtained from electrical conductivity measurements [16,17], electron paramagnetic resonance [18–20], optical measurements [7,8], scanning tunneling microscopy, and spectroscopy [21] as well as infrared spectroscopy [22]. On the other hand, first-principles calculations based on density functional theory (DFT) provide a robust and complementary approach for gaining information about polaron properties [23–28]. This includes binding and migration energies [28], photoluminescence peaks [21,29], lattice distortions around localized charge, and contributing modes responsible for the trapping mechanism [30].

$PbTiO_3$ is a prototypical ABO_3 ferroelectric with a ferroelectric-to-paraelectric phase transition at about 763 K [31,32]. $PbTiO_3$ is also the end member of the most important and widely used piezoelectric and ferroelectric solid solutions, including $Pb(Zr_xTi_{1-x})O_3$ and $Pb(Mg_{1/3}Nb_{2/3})O_3$-$PbTiO_3$ ceramics [33]. These materials have applications ranging from nonvolatile electronic and optical storage memory devices to high-strain actuators. Due to its technological importance, the defect chemistry of $PbTiO_3$ including native defects [34–38], aliovalent doping [39–43], and defect dipoles [43–46] has been intensively investigated, both theoretically and experimentally. Nevertheless, the state of understanding of polarons in this material is relatively poor. Considering the influence of trapped charges on generating an internal bias field and the respective impact on polarization and pinning of ferroelectric domain walls, the identification of such quasiparticles in this model ferroelectric perovskite oxide is of high interest.

In 1993, Robertson *et al.* used electron paramagnetic resonance measurements to study charge trapping in $Pb(Zr_xTi_{1-x})O_3$ ferroelectric compositions [47]. According to their report, the paramagnetic Pb^{3+} hole center is present in all samples independent of composition. The Ti^{3+} electron

*ghorbani@mm.tu-darmstadt.de

center, however, is only seen in a narrow range of compositions around $x = 0.5$ [47,48]. Later, Eglitis *et al.* [9] studied the presence of self-trapped electrons (STels) in cubic (paraelectric phase) $PbTiO_3$ by a semiempirical Hartree-Fock method and attributed the green-luminescence signal at 2.38 eV to the presence of $Ti^{+}3$ electron polarons with a binding energy of 0.22 eV . In 2014, Erhart *et al.* [26] investigated the formation of self-trapped holes (STHs) in cubic $PbTiO_3$ using the DFT+U formalism and found that the formation of STHs in $PbTiO_3$ is not energetically favorable. This finding has been rationalized by considering the strong coupling between Pb 6s and O 2p states near the valence band maximum (VBM) of $PbTiO_3$, which results in a higher VBM in this material compared to other perovskites [49] forming STHs on O 2p sites [26,50].

Despite the technological importance of the tetragonal ferroelectric phase of $PbTiO_3$, only a very small number of studies attempted to study polarons in this material. As a result, the current understanding of the behavior of excess charges in $PbTiO_3$ is very limited. At this point, *ab initio* calculations can shape our knowledge to a great extent, since they allow us to have a quantitative understanding of the trapping energy and migration barrier of self-trapped charge carriers. To this end, we systematically quantify the errors in the calculated polaron trapping energy associated with the computational approach. Using the DFT+U method [51], we first evaluate the suitability of different U parameters for correcting the DFT self-interaction error in the polaron configuration. We then compare polaron binding energies obtained with different k-point grids. Next, we study how cell parameters obtained through relaxation with different functionals influence the trapping energy of the polaron. In a next step, we analyze band structures, trapping energies, and migration barriers of self-trapped electrons on Ti, using three different projector augmented wave (PAW) setups for Ti. Using hybrid functional calculations we finally construct a configuration coordinate diagram to provide a theoretical prediction of the photoluminescence features associated with the identified STel.

II. THEORETICAL APPROACH

Calculations in the framework of DFT were carried out using the Vienna *Ab initio* Simulation Package [52,53]. The interactions between the ionic cores and the valence electrons were described with the PAW approach [54,55]. Calculations were performed using a $3 \times 3 \times 3$ supercell containing 135 atoms. To test the influence of the Ti pseudopotential on our calculations, the following three different PAW setups were considered: Ti 4s and 3d orbitals as valence states with a total number of 4 valence electrons; Ti 3p, 4s, and 3d orbitals as valence states with a total number of 10 valence electrons; and Ti 3s, 3p, 4s, and 3d orbitals as valence states with a total number of 12 valence electrons. The convergency of the cutoff energy was tested for all three PAW setups and the results confirm that a plane-wave cutoff energy of 400 eV is converged for all cases. The convergence threshold for electronic self-consistency was set to 10^{-6} eV. The Perdew-Burke-Ernzerhof (PBE) exchange-correlation functional [56] was employed.

TABLE I. Calculated and experimentally measured lattice parameters a and c/a and energy band gap E_g for $PbTiO_3$.

	a (Å)	c/a	E_g (eV)
PBE	3.84	1.23	2.41
PBE + U	3.98	1.005	2.21
HSE	3.89	1.06	2.95
Expt.	3.89 [62]	1.07 [62]	3.6 [63]

It is well established that DFT based on semilocal exchange-correlation functionals suffers severely from self-interaction errors. As a consequence, the electron interacts with itself, which favors its artificial delocalization. This results in sizable errors in describing strongly localized states of polarons [25,57–59]. Therefore, in order to obtain an accurate quantitative and qualitative description of the total energy and structural properties of the polaron configuration, applying a functional that can treat the self-interaction error of the density functional approximations is essential. For correcting the DFT self-interaction error, we employed DFT+U and hybrid functional approaches [60]. In the DFT+U calculations, we used a U parameter of 4.75 eV on the Ti d orbital, as suggested by Gou *et al.* [61].

We note that this choice of $U = 4.75$ eV also results in a polaron binding energy being consistent with the HSE06 functional.

The hybrid functional calculations were performed using the HSE06 formalism [60], where the contribution of screened Hartree-Fock exchange was set to the standard value of $\alpha = 0.25$ and the screening range of the electron interaction was treated by setting the screening parameter, w, to 0.20 $Å^{-1}$. Relaxation of the ionic positions was continued until the residual Hellmann-Feynman force component on each ion fell below 0.01 eV/Å . The obtained lattice parameters for the unit cell of $PbTiO_3$ and the electronic band-gap energy are listed in Table I.

Table I show that the PBE functional tends to overestimate the tetragonality of $PbTiO_3$. On the other hand, the lattice relaxation with the PBE + U functional takes the structure back to a nearly cubic lattice with a c/a ratio of 1.005 and subsequently underestimates ferroelectric distortions. The lattice parameters obtained with the HSE functional are in very good agreement with experimental results. Although the band-gap energy obtained with HSE06 is smaller than with PBE0 [61], we performed our calculations with HSE06 because the lattice parameters obtained with HSE06 are described very accurately.

An important feature of a polaron is its trapping energy, which can be calculated using the expression

$$E_{\text{trap}}^{\pm 1} = E_{\text{pol}}^{\pm 1} - E_{\text{id}}^{\pm 1} + \Delta E_{\text{corr}}(q = \pm 1), \tag{1}$$

where $E_{\text{pol}}^{\pm 1}$ and $E_{\text{id}}^{\pm 1}$ are the total energies of supercells corresponding to the polaron and the perfect system, respectively. In practice, calculating $E_{\text{pol}}^{\pm 1}$ consists of taking the system out of a high-symmetry configuration through applying an initial symmetry-breaking distortion followed by structure relaxation in the singly charged supercell. The term $\Delta E_{\text{corr}}(q = \pm 1)$ accounts for the correction of the artificial image charge

TABLE II. Calculated macroscopic dielectric tensor of tetragonal $PbTiO_3$. ε_∞ and ε_{ion} are electronic and ionic contributions to the dielectric tensor, respectively, and ε denotes the static dielectric constant. The experimental values are given in parentheses.

Lattice direction	ε_∞	ε_{ion}	ε
a	316.0 (210 [65])	7.1	323.1
b	375.3	7.1	382.4
c	123.7 (115 [65])	6.9	130.6

interactions in polaron supercells. Although both $E_{\text{pol}}^{\pm 1}$ and $E_{\text{id}}^{\pm 1}$ configurations are equally charged, spurious image charge interactions exist only in the polaron system, while the delocalized charge in the ideal supercell will be compensated by the existing jellium background charge. The leading (first-order) correction term for the electrostatic interaction energy between the images of charged supercells is the screened Madelung energy [64]:

$$\Delta E_{\text{corr}}(q) = \frac{2}{3}\frac{Mq^2}{2\varepsilon L}, \tag{2}$$

where M is the lattice-dependent Madelung constant, L is the length of the supercell, and ε is the static dielectric constant of the host, which has been obtained by computing the dielectric tensor from the system's response to a finite external field under absence (electronic contribution, ε_∞) and presence (ionic contribution, ε_{ion}) of lattice distortions. The sum of the ε_∞ and ε_{ion} terms yields the ε. Using DFT+U, we obtained ε_∞ and ε_{ion} as listed in Table II. Due to the large dielectric response of $PbTiO_3$ (both experimentally and computationally), the image-charge correction term has not been taken into account. The deviation between the calculated dielectric constant (316.0) and the experimental value (210) for the electronic contribution is large. The problem is probably linked to the exchange-correlation functional which results in a band-gap energy that is about 40% smaller than the experimental energy gap in this material. Furthermore, other aspects such as temperature, pressure, impurities, defects, and surface charges can affect the experimental results [66–68]. $SrTiO_3$, for instance, has a dielectric constant of ∼300 at room temperature, which increases to ∼30 000 close to 0 K [69]. And in $BaTiO_3$, the dielectric constant ranges from 500 to 6900, depending on the synthesis technique [70].

For investigating the polaron dynamics, we used a linear interpolation scheme to construct a hopping trajectory between two neighboring polaronic configurations, where an electron polaron localized at a Ti^{3+} site jumps to a neighboring Ti^{4+} site. The energy barrier for the transition of the polaron was then characterized using the nudged elastic band approach [71,72].

III. RESULTS AND DISCUSSIONS

A. PBE + U calculations

The stability of a polaron can be understood by considering its trapping energy. While a positive trapping energy manifests instability of the polaronic configuration, a negative trapping energy means that the polaronic configuration is energetically more stable than the delocalized solution. Hence, the system prefers to relax into the polaronic solution. We studied the trapping of a positive charge (STH) on oxygen 2p orbitals and a negative charge on Ti 3d orbitals. In case of the STH, we obtained positive trapping energy, which is consistent with the report of Erhart *et al.* on the formation of STHs in cubic $PbTiO_3$ [26]. This finding implies that the localized holes (STHs) are energetically less favorable than their delocalized counterparts. Therefore, small polaron formation by hole self-trapping on O 2p is metastable and energetically hindered. Note that we did not study other small hole polaron mechanisms, such as bound polarons close to an acceptor defect. Both Geneste *et al.* and Sun *et al.* have studied the interaction of polarons with dopants in $BaSnO_3$ and oxygen vacancies in CeO_2, showing that the interaction with point defects can stabilize polarons [50,73]. Therefore, existence of hole polarons in this material cannot be ruled out. For the STel, we observed a negative trapping energy revealing the tendency of the system towards trapping excess electrons on Ti sites. Figure 1 illustrates the atomic configuration and charge distribution of the STel in $PbTiO_3$, where the STel is mainly localized on the Ti d_{xy} orbital.

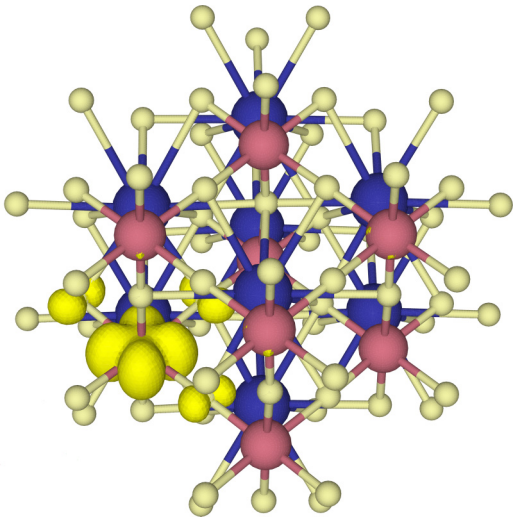

FIG. 1. The relaxed configuration of the STel on Ti site in $PbTiO_3$. The blue, pink, and yellow spheres represent Pb, Ti, and O ions, respectively. The charge density isosurface illustrates the polaron wave function.

To ensure the reliability of the computational procedure, we tested the dependence of the calculated trapping energy on the k-point grid, lattice constant, and PAW setup. So far, the main focus was given to an accurate description of the on-site localization parameter (Hubbard U, Fock exchange, etc). For obtaining an accurate polaron trapping energy, as will be shown in the following, an accurate determination of the k-point mesh, lattice constant, and elemental PAW setups are essential and as important. Indeed, different lattice parameters and PAW setups can drastically affect the polaron binding energy and lead to wrong conclusions, as will be discussed below.

We first focus on the effect of the k-point sampling on the polaron trapping energy. In Table III, trapping energies

TABLE III. Trapping energies of STel in $PbTiO_3$ using different Γ-centered k grids. The calculations were carried out with PBE + U [UTi($3d$) = 4.75 eV].

2 × 2 × 2	3 × 3 × 3	4 × 4 × 4	5 × 5 × 5
–0.12	–0.19	–0.18	–0.18

of the STel using different k-mesh sets are listed. According to Eq. (1), the trapping energy is obtained as the difference in total energy of a supercell of a perfect crystal containing an extra electron in the conduction band and the total energy of a supercell with the localized electron. While the supercell containing the STel possesses only fully occupied and fully empty (spin-polarized) states, the ideal supercell with excess charge has partial occupancies in its electronic states. Hence, its total energy converges slower as a function of the k mesh. Consequently, the convergence of the trapping energy with respect to the k-point density should be tested. Previously, Erhart *et al.* [26] studied the convergence of formation energy of STHs in $SrTiO_3$ with different k meshes using Eq. (1) and the formation energy relation from defect thermodynamics. Their results demonstrate that convergence is slower when using Eq. (1) and as a consequence higher k-mesh grids need to be applied. It is clear from Table III that the magnitude of the trapping energy depends on the size of the k mesh and that the commonly considered 2 × 2 × 2 k mesh for the 3 × 3 × 3 perovskite-based supercells is not a precise choice and the trapping energy is converged already for a 4 × 4 × 4 k mesh. Note that the difference of trapping energies calculated using a 2 × 2 × 2 and a 4 × 4 × 4 k mesh is 60 meV. This significant difference underlines the importance of using a k mesh that ensures a converged trapping energy. Accordingly, the rest of the calculations presented in this paper were performed using a 4 × 4 × 4 Γ-centered k mesh.

In order to find other sources for the variation of the polaron trapping energy, we carried out a detailed benchmarking considering the effects of lattice parameters and PAW setups. As mentioned in the previous section and shown in Table I, the PBE functional tends to magnify the c/a ratio of the tetragonal $PbTiO_3$. On the other hand, by applying the U parameter, the relaxed structure becomes almost cubic, exhibiting a minimal ferroelectric distortion. For studying the effect of lattice parameters on the polaron trapping energy, we constructed 3 × 3 × 3 supercells from conventional unit cells and used PBE, HSE, as well as experimental lattice constants. Hereafter, @PBE, @HSE and @Exp refer to the PBE + U calculations performed respectively on the supercells constructed with PBE, HSE, and experimental lattice parameters. Next, we tested the influence of the Ti PAW setup on the polaron trapping energy. We note that PAW implementations usually rely on the frozen-core approximation, which is based on separating the electrons into core and valence electrons. In this method, the electrons in the core orbitals are not allowed to polarize under the effect of the valence electrons or the other atoms, which makes this method distinct from an all-electron method [74]. Keeping this in mind, we decided to quantify the effect of the PAW setups on electronic structure calculations of small polarons. Here, calculations were first

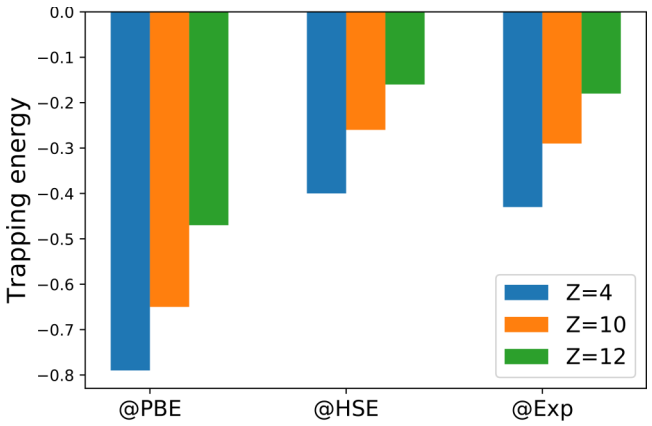

FIG. 2. Calculated trapping energies of STel on Ti atom obtained with PBE + U, using different PPs of Ti. Z denotes the number of electrons treated as valence electrons in the PP of Ti. @PBE, @HSE, and @Exp denote PBE + U calculations performed with PBE, HSE, and experimental lattice constants, respectively. Calculations were carried out using 4 × 4 × 4 Γ-centered grids.

performed by treating Ti 4s and 3d orbitals as valence states with 4 total valence electrons (Z = 4, large core) on the Ti site. Then, Ti 3p, 4s, and 3d orbitals with a total number of 10 electrons (Z = 10, medium core) were considered as valence electrons. Finally, the trapping energy was calculated by treating Ti 3s, 3p, 4s, and 3d orbitals as valence states with a total number of 12 valence electrons (Z = 12, small core) on Ti. The results are illustrated in Fig. 2.

According to Fig. 2, the trapping energy obtained for supercells constructed from the PBE-relaxed unit cell (@PBE) is much more negative than those obtained with @HSE and @Exp supercells. This is because the larger c/a ratio in @PBE calculations allows for more ionic relaxations and stronger localization, leading to more negative trapping energies. In particular, in the case of Z = 4, the trapping energy of the STel varies from –0.79 eV using the @PBE supercell to –0.40 eV and –0.43 eV using the @HSE and @Exp supercells, respectively.

Note that in all calculations the trapping energy is a negative number, which speaks for formation of STels. However, the large variation of polaron trapping energy in different supercells may impact the polaron hopping mechanism. This can impact the polaron mobility and spatial configuration at different temperatures. Hence, to ensure reliable ionic relaxation and charge localization, we considered @Exp supercells for our further analysis with the PBE + U, and used @HSE supercells for our calculations with the HSE functional. Note that, according to Fig. 2, PBE + U calculations using @HSE and @Exp supercells yield very similar results.

For computational efficiency, it is often desirable to employ pseudopotentials (PPs) with the least number of electrons considered as valence electrons. While this "standard" choice of PP decreases the computational time, it is instructive to examine its fidelity more closely. So, the question that we address here is how or whether the inclusion of semicore levels in PP would affect the trapping energy and diffusion barrier of small polarons. To that end, we performed calculations

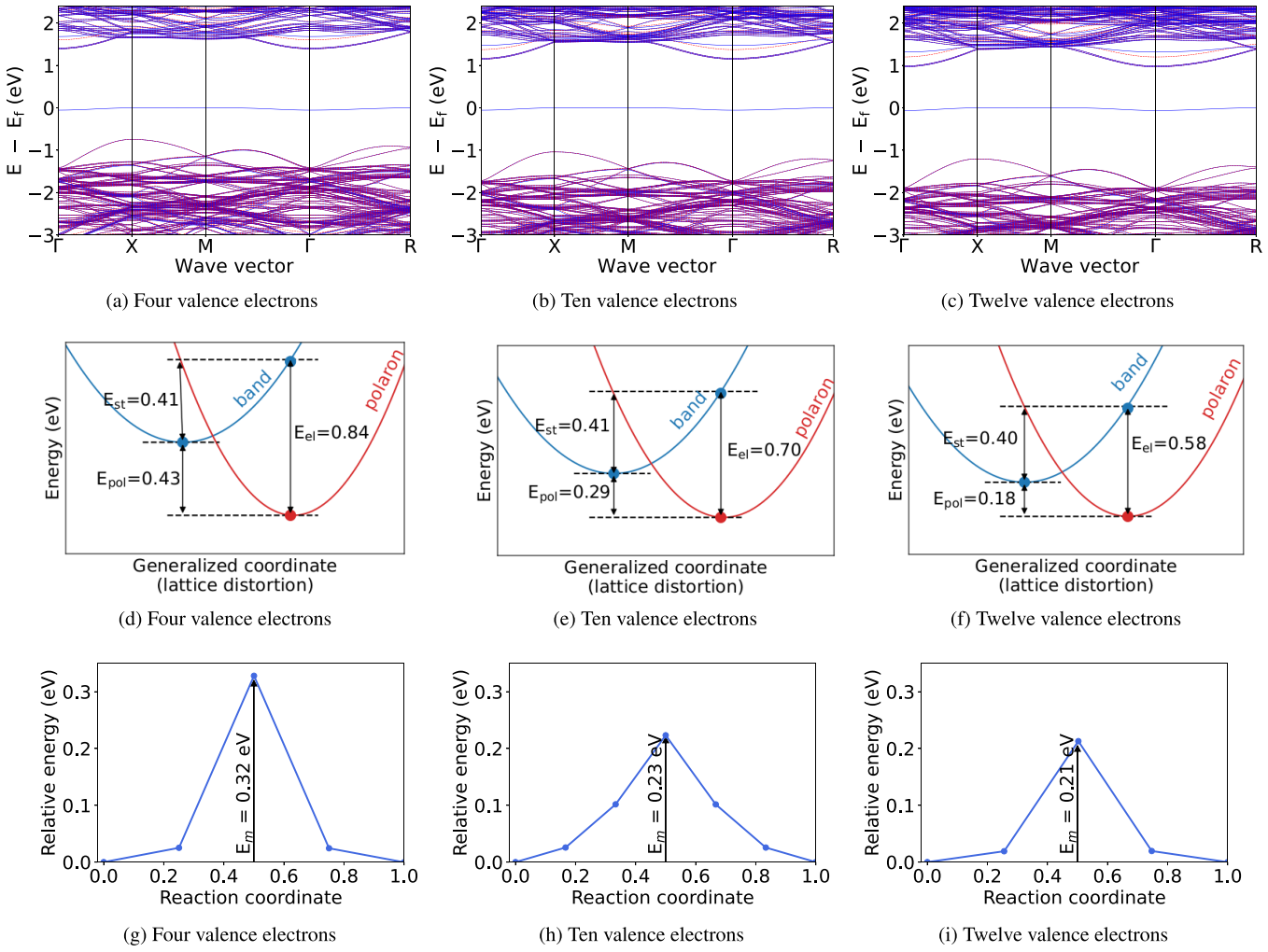

(a) Four valence electrons (b) Ten valence electrons (c) Twelve valence electrons

(d) Four valence electrons (e) Ten valence electrons (f) Twelve valence electrons

(g) Four valence electrons (h) Ten valence electrons (i) Twelve valence electrons

FIG. 3. Top row: Electronic band structure of polaronic configuration, calculated by treating (a) 4, (b) 10, and (c) 12 outermost electrons of Ti as valence. Middle row: The schematic configuration coordinate diagram depicting the excitation of a small STel to a delocalized electron configuration energy as a functional of lattice distortion, calculated by treating (d) 4, (e) 10, and (f) 12 outermost electrons of Ti as valence. Bottom row: Schematic configuration coordinate diagram depicting the excitation of a small STel to a nearest-neighbor site, calculated by treating (g) 4, (h) 10, and (i) 12 outermost electrons of Ti as valence.

treating 4, 10, and 12 electrons of Ti as valence electrons. With these setups, the comparison clearly demonstrates that the fewer valence electrons in the PAW setup, the more negative will be the trapping energy of the polaron. For example, the trapping energy for @Exp calculations changes from -0.43 to -0.18 eV when going from a large-core ($Z = 4$) to a small-core ($Z = 12$) PP scheme, as can be seen in Fig. 2. For a closer inspection of this behavior, we compared electronic band structures and configuration coordinate diagrams for the three PP setups using a $4 \times 4 \times 4$ k mesh and @Exp supercell. The results are shown in Fig. 3.

The PBE + U spin-polarized band structure of $PbTiO_3$ shows one fully occupied flat band in the spin-up channel within the band gap for all three sets of calculations [see Figs. 3(a)–3(c)]. The flat band shows almost no dispersion, the relevant feature of a fully localized state. The precise placement of the flat band (polaronic band), however, changes with the applied PP. The flat bands for $Z = 4$, 10, and 12 are 1.39, 1.15, and 0.96 eV below the conduction-band minimum, respectively.

Next, to inspect the source of variation in polaron trapping energies consequent to applying different PPs, schematic configuration coordinate diagrams [27,75,76] were calculated for the three PP setups and are illustrated in Figs. 3(d)–3(f). The polaron trapping energy can be decomposed into strain energy and electronic energy. The strain energy (E_{st}), being a positive number, corresponds to the relaxation energy gain for distorting the lattice and stabilizing the localized charge configuration. The electronic energy (E_{el}), being a negative number, is the energy cost by localizing the electron at the Ti site. The electronic energy E_{el} is also indicative of the energy required for exciting a carrier from a localized in-gap state to a delocalized band state and corresponds to the absorption of a photon of that energy for making the transition from the localized to the delocalized state plausible. Note that the electronic energy E_{el} can be measured in photoemission spectroscopy or scanning tunneling spectroscopy and then can be directly compared to the theoretical value [21,29,77].

We found that the strain energy E_{st} is similar in all three calculations. This is consistent with the relaxation patterns,

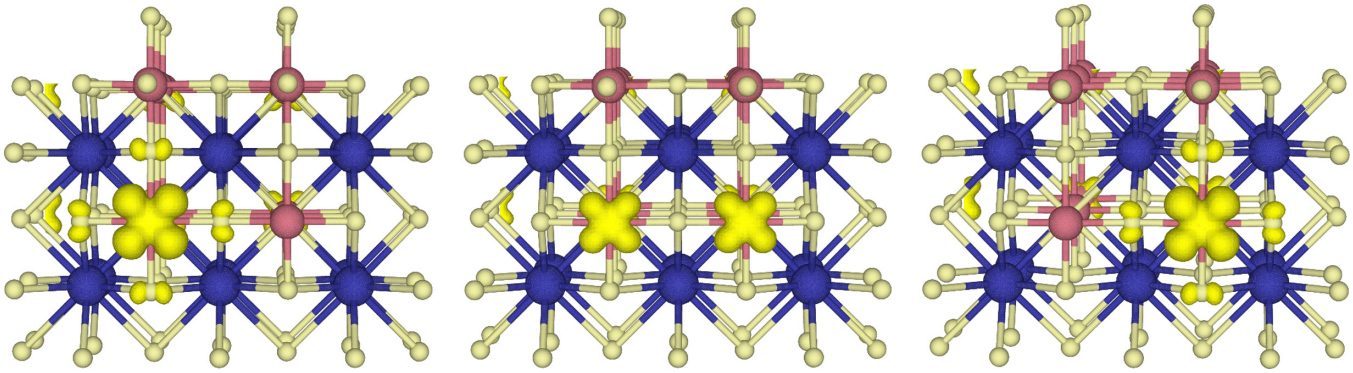

(a) Initial configuration (b) Saddle configuration (c) Final configuration

FIG. 4. Charge distribution corresponding to the small STel hopping from the (a)initial to the (b) saddle point, and (c) final configurations using PBE + U calculations.

which are similar for the three calculations, all showing analogous outward relaxation of O atoms in the xy plane. So, the difference in polaron trapping energies stems from the electronic part, which decreases considerably when moving from 4 to 12 valence electrons on Ti sites. This inconsistency can arise from the interactions between the Ti d-level and the semicore states, as the localized d orbitals are more tightly bound to the semicore states. We will discuss this feature at the end of the current section.

Next, we studied the change in the migration barrier of the STel using the three PP setups [Figs. 3(g)–3(i)]. The corresponding charge distributions for the STel hopping at the initial, saddle point, and final configurations are shown in Fig. 4. Here, the excitation of the STel is considered through hopping from its self-trapping potential well to an adjacent site, separated by 3.90 Å. In the initial configuration, the extra electron is localized on one particular Ti site, while all other Ti atoms are in a 4+ oxidation state, Ti^{3+}-Ti^{4+}. In the final configuration, the electron hopped to an adjacent site, leaving the original Ti site and reducing the oxidation state of the next Ti ion, Ti^{4+}-Ti^{3+}. The migration barrier is shown as E_m. Our calculations indicate that when going from a large-core PP to a small-core PP, the migration barrier changes from 320 to 210 meV, amounting to a large variation of 110 meV. This provides evidence that the migration barrier is also highly sensitive to the choice of the PP and a large-core scheme is insufficient for obtaining a correct migration barrier, E_m.

As shown in Fig. 4(b), at the transition state, the excess electron is equally distributed between the initial and final states. This feature holds for all three PP setups and is an indication of an adiabatic transfer of excess electron from one Ti site to the neighboring Ti site [72]. In adiabatic hopping, there is a strong electronic coupling between the initial and final states, leading to a gradual transfer of electron from one site to the other, and a migration barrier which is generally smaller than the polaron trapping energy. As a result, the polaron transport proceeds through thermal hopping without delocalization [78]. We see in Figs. 3(g)–3(i) that, as a result of semicore relaxation, the migration barrier decreases by including semicore levels in the Nudged Elastic Band (NEB) calculations. For $Z = 4$ and 10, the polaron migration barrier is smaller compared to the polaron trapping energy. For $Z = 12$, however, the migration barrier becomes slightly larger than the trapping energy. This implies that the polaron hops through a delocalization-localization mechanism. However, since the migration barrier is only 0.03 eV larger than the polaron trapping energy, this slight surplus could be an artifact of the PBE+U functional. It is important to note that the DFT+U tends to underestimate coupling between the initial and final configurations and consequently the activation barrier for polaronic hopping is commonly overestimated when applying DFT+U [73]. The estimation can be improved by using more accurate but substantially more expensive HSE06 hybrid functional.

The effects of the semicore levels relaxation on the polaron migration barrier has been also investigated in $FePO_4$ by Wang *et al.* [79]. Their results show that the relaxation of electronic states far below the Fermi energy could impact the *ab initio* polaronic migration barrier substantially. To have a closer look at the effect of semicore level electronic relaxation on polaron trapping energy and the migration barrier, the projected density of states of the Ti orbitals in the presence of a delocalized electron and a STel are presented in Fig. 5. The results show that the electronic interactions between the localized d state of the polaron and the semicore states [Fig. 5(b)] breaks the symmetry and induces degeneracy of the Ti $3p$ (the blue lines between −30 and −40 eV) and $3s$ (the green lines between −50 and −60 eV) states, a feature that does not exist while having a delocalized electron in the system [Fig. 5(a)]. Hence, the localized electron on the Ti d orbital gives rise to additional electronic relaxations on electronic levels far below the Fermi energy. So, the inclusion of the semicore states in the calculations allows for the full electronic relaxations of the semicore states. As a result, the total energy of the system and, in consequence, the trapping energy and migration barrier of the polaron decrease. Note that when the semicore states are taken as frozen states, such electronic relaxations are not allowed anymore and their significant contribution to the trapping energy and the migration barrier of polaron will be neglected.

B. Hybrid functional calculations

As mentioned before, the current state of the art of the polarons in tetragonal $PbTiO_3$ is not well understood and,

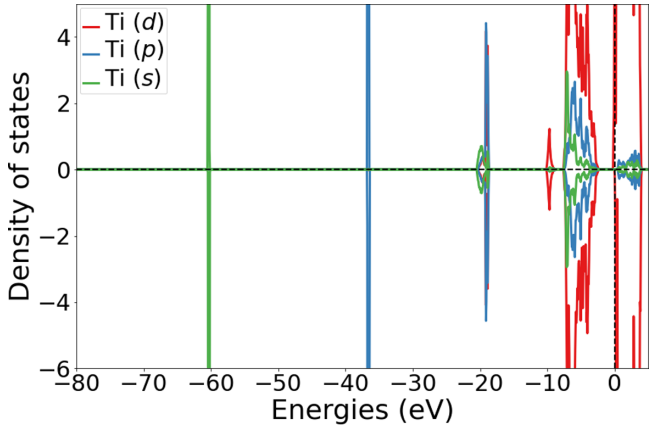

(a) Band electron

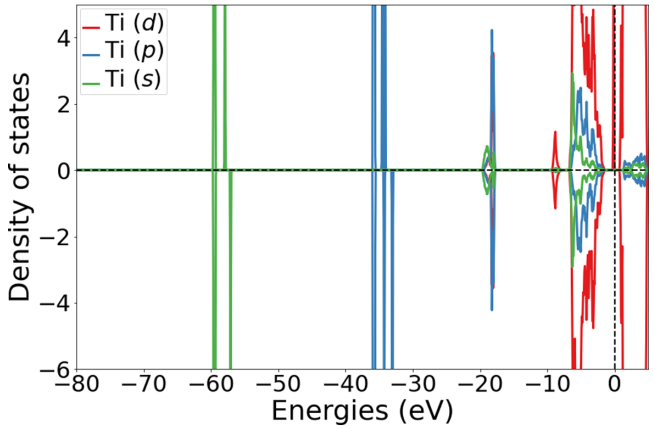

(b) Self-trapped electron

FIG. 5. Spin-polarized projected density of states of Ti ions for two configurations: (a) The added electron is delocalized, forming a band electron, and (b) the added electron is localized on a Ti site, forming a STel.

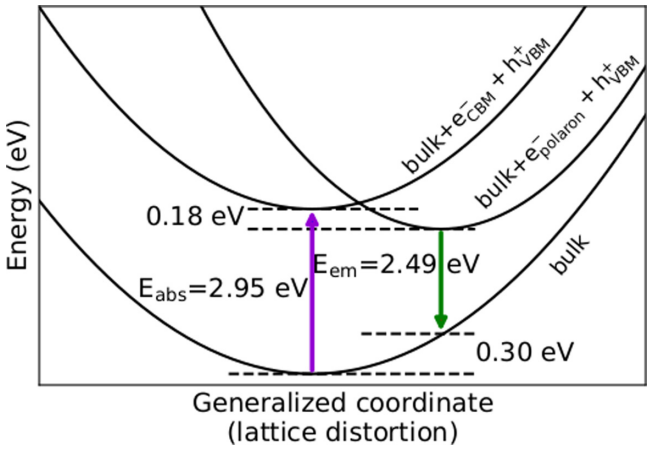

FIG. 6. Schematic configuration coordinate diagram showing the optical absorption process, associated with the STel in $PbTiO_3$.

despite its technological importance, there is only very little known about polarons in this material. We are only aware of one Electron Paramagnetic Resonance (EPR) study performed by Robertson *et al.* [48], where electron polarons associated with Ti^{3+} centers were reported in tetragonal $Pb(Zr_xTi_{1-x})O_3$, only around $x = 0.5$. However, they could not find evidence for the existence of Ti^{3+} centers in other compositions with varying x. This contrasts with our results, where both PBE+U and HSE06 calculations provide strong evidence for the existence of electron polarons on Ti d orbitals of pure tetragonal $PbTiO_3$. The discrepancy between the experimental and theoretical studies can be related to the lifetime of the excited state. The EPR measurements are performed in an optically excited state and optical excitation always comes along with recombination. So, the faster the recombination, the lower the polaron concentration. Thus, it is probably the lifetime of the excited state, which is higher in $Pb(Zr_xTi_{1-x})O_3$ than in pure $PbTiO_3$.

The results presented in the current section were calculated using the HSE06 hybrid functional. The lattice parameters were also relaxed using the HSE06 functional. Here, we first compare the results obtained using the PBE + U (UTi($3d$) = 4.75 eV @Exp lattice constants) functional to those attained with the HSE06 hybrid functional. Using a $4 \times 4 \times 4$ Γ-centered k mesh, the HSE06 STel trapping energies obtained with large-, medium-, and small-core PAW setups are respectively -0.41, -0.30, and -0.16 eV. Note that the HSE06 calculated trapping energies are in very good agreement with those obtained with PBE + U. Note that applying various PAW setups has a large influence over the calculated trapping energies, here as well. This reveals that there are significant electronic interactions between the polaronic d state and the semicore states, which would not be taken into consideration if the semicore levels are treated as frozen core states. Therefore, in studying polarons, and irrespective of the applied functional, the semicore states must be treated as valence electrons.

Since HSE06 calculations yield a good estimate of the electronic band gap of $PbTiO_3$, we are able to analyze the optical transitions associated with the STel. The configuration coordinate diagram illustrating the absorption and luminescence processes associated with the small STel in $PbTiO_3$ is given in Fig. 6. The lowest parabola denotes the bulk, the highest parabola denotes the bulk with an pair, and the middle parabola denotes the bulk with a STel. Absorption of photons with energies equal to or larger than the band gap produces an electron-hole pair, as shown with the upward-pointing violet arrow. The photogenerated electron goes through a phonon-mediated nonradiative process and gets trapped on a Ti site. Radiative recombination of the valence-band hole with the STel results in a below-gap emission (or photoluminescence) peak in the optical transition spectra in photoluminescence and cathodoluminescence measurements, which is associated with emitting a photon and is shown with the downward-pointing green arrow. Finally, the lattice gets back to its ground-state (bulk) configuration through a phonon-mediated relaxation.

Conventionally, luminescence of wide-gap materials has been attributed to the presence of intrinsic defects or dopants. However, for many perovskites including $SrTiO_3$, $BaTiO_3$, and $PbTiO_3$ the optical measurements indicate broad band emission in the visible spectral region ("green" luminescence), which could not be associated to any defect or

impurity states and could be only explained by considering the existence of an electron polaron on the Ti site. According to these experiments, the emission spectra in all of these perovskites peaks around 2.4 eV [10,80,81]. For $PbTiO_3$, our calculated STel emission of 2.49 eV explains the green luminescence in this material, in agreement with previous experiments.

IV. CONCLUSIONS

$PbTiO_3$ is a prototypical ABO_3 ferroelectric material, which is also the end member of several of the most important piezoelectric and ferroelectric solid solutions. Nevertheless, the formation and migration of small polarons on its technologically important tetragonal phase are missing in the literature. Using a Hubbard U parameter of 4.75 eV on a Ti d orbital, a $4 \times 4 \times 4$ Γ-centered k mesh, and the small-core PP of Ti, we identified the formation of a small STel with the trapping energy of 0.18 eV, which was in very good agreement with results obtained with the HSE06 functional (0.16 eV). Furthermore, we have investigated the migration of the STel using the nudged elastic band, resulting in a migration barrier of 0.21 eV, which is too high to have significant influence on the n-type conductivity of $PbTiO_3$.

We also present the configuration coordinate diagram illustrating energy balance as a function of lattice distortions for delocalized and polaronic solutions and predict the energy required to absorb a photon for exciting an electron from a localized in-gap state to a delocalized band state to be 0.58 eV. Complementary insights on the optical transitions of the electron polaron were provided through calculating the schematic configuration coordinate diagram associated with the optical transitions of the STel using hybrid functional calculations. The results showed that recombination of the STel with a free hole in the valence band leads to an emission peak at 2.49 eV, giving rise to a green luminescence and in good agreement with the experimental optical emission peak at 2.4 eV. For the case of hole self-trapping on O $2p$, we found that the localized holes are energetically less favorable than their delocalized counterparts.

In terms of the methodology, we presented a systematic benchmark of the effect of k-mesh grids, lattice parameters, and PP on polaron trapping energy in $PbTiO_3$ using density functional theory calculations. So far, an accurate description of the on-site localization parameter (U, Fock exchange, etc.) received the most attention for a proper description of polarons in materials of study. For obtaining an accurate polaron trapping energy, however, we show that a correct determination of the k-point mesh, lattice constant, and elemental PAW setups are as essential and can drastically affect the polaron binding energy. Our results showed that the magnitude of the polaron trapping energy and migration barrier is highly sensitive to the choice of the PP, and to a less extent to the choice of lattice parameters and k-mesh grid. In view of the present results, we conclude that in order to properly quantify polaron properties, the effects of choosing a PP need to be taken into account in future studies and the precision of calculations cannot be sacrificed by lowering the computational cost.

ACKNOWLEDGMENTS

This work was supported by the LOEWE program of the State of Hesse, Germany, within the project FLAME (Fermi Level Engineering of Antiferroelectric Materials for Energy Storage and Insulation Systems). The authors gratefully acknowledge the computing time provided to them on the high-performance computer Lichtenberg at the NHR Centers NHR4CES at TU Darmstadt. This is funded by the Federal Ministry of Education and Research, and the state governments participating on the basis of the resolutions of the GWK for national high performance computing at universities. The calculations for this research were conducted with computing resources under the project 01316.

[1] J. B. Varley, A. Janotti, C. Franchini, and C. G. Van de Walle, Phys. Rev. B **85**, 081109(R) (2012).
[2] B. Faust, H. Müller, and O. F. Schirmer, Ferroelectrics **153**, 297 (1994).
[3] J. Yue, N. F. Quackenbush, I. Laraib, H. Carfagno, S. Hameed, A. Prakash, L. R. Thoutam, J. M. Ablett, T.-L. Lee, M. Greven, M. F. Doty, A. Janotti, and B. Jalan, Phys. Rev. Mater. **4**, 112001(R) (2020).
[4] F. Ambrosio, J. Wiktor, F. De Angelis, and A. Pasquarello, Energy Environ. Sci. **11**, 101 (2018).
[5] F. Ambrosio and J. Wiktor, J. Phys. Chem. Lett. **10**, 7113 (2019).
[6] M. Friedrich, W. G. Schmidt, A. Schindlmayr, and S. Sanna, Phys. Rev. Materials **1**, 054406 (2017).
[7] O. F. Schirmer, J. Phys.: Condens. Matter **18**, R667 (2006).
[8] O. F. Schirmer, M. Imlau, C. Merschjann, and B. Schoke, J. Phys.: Condens. Matter **21**, 123201 (2009).
[9] R. I. Eglitis, E. A. Kotomin, V. A. Trepakov, S. E. Kapphan, and G. Borstel, J. Phys.: Condens. Matter **14**, L647 (2002).
[10] R. I. Eglitis, E. A. Kotomin, and G. Borstel, J. Phys.: Condens. Matter **14**, 3735 (2002).
[11] E. A. Kotomin, R. I. Eglitis, A. V. Postnikov, G. Borstel, and N. E. Christensen, Phys. Rev. B **60**, 1 (1999).
[12] V. S. Vikhnin, R. I. Eglitis, S. E. Kapphan, G. Borstel, and E. A. Kotomin, Phys. Rev. B **65**, 104304 (2002).
[13] N. S. Bein, P. Machado, M. Coll, F. Chen, M. Makarovic, T. Rojac, and A. Klein, J. Phys. Chem. Lett. **10**, 7071 (2019).
[14] C. Lohaus, A. Klein, and W. Jaegermann, Nat. Commun. **9**, 4309 (2018).
[15] Y. Hermans, A. Klein, H. P. Sarker, M. N. Huda, H. Junge, T. Toupance, and W. Jaegermann, Adv. Funct. Mater. **30**, 1910432 (2020).
[16] P. Nagels, M. Denayer, and J. Devreese, Solid State Commun. **1**, 35 (1963).
[17] H. Ihrig, J. Phys. C **9**, 3469 (1976).
[18] H. Kauppinen, L. Baroux, K. Saarinen, C. Corbel, and P. Hautojärvi, J. Phys.: Condens. Matter **9**, 5495 (1997).

[19] E. Possenriede, H. Kröse, T. Varnhorst, R. Scharfschwerdt, and O. F. Schirmer, Ferroelectrics **151**, 199 (1994).

[20] S. Yang, A. T. Brant, N. C. Giles, and L. E. Halliburton, Phys. Rev. B **87**, 125201 (2013).

[21] M. Setvin, C. Franchini, X. Hao, M. Schmid, A. Janotti, M. Kaltak, C. G. Van de Walle, G. Kresse, and U. Diebold, Phys. Rev. Lett. **113**, 086402 (2014).

[22] H. Sezen, H. Shang, F. Bebensee, C. Yang, M. Buchholz, A. Nefedov, S. Heissler, C. Carbogno, M. Scheffler, P. Rinke, and C. Wöll, Nat. Commun. **6**, 6901 (2015).

[23] S. Lany, Phys. Status Solidi B **248**, 1052 (2011).

[24] J. A. Chan, S. Lany, and A. Zunger, Phys. Rev. Lett. **103**, 016404 (2009).

[25] S. Lany and A. Zunger, Phys. Rev. B **80**, 085202 (2009).

[26] P. Erhart, A. Klein, D. Åberg, and B. Sadigh, Phys. Rev. B **90**, 035204 (2014).

[27] S. Lany, J. Phys.: Condens. Matter **27**, 283203 (2015).

[28] A. Lindman, P. Erhart, and G. Wahnström, Phys. Rev. B **94**, 075204 (2016).

[29] A. Janotti, C. Franchini, J. B. Varley, G. Kresse, and C. G. Van de Walle, Phys. Status Solidi RRL **7**, 199 (2013).

[30] E. Bousquet, H. Hamdi, P. Aguado-Puente, E. K. H. Salje, E. Artacho, and P. Ghosez, Phys. Rev. Research **2**, 012052(R) (2020).

[31] S. A. Mabud and A. M. Glazer, J. Appl. Crystallogr. **12**, 49 (1979).

[32] R. E. Cohen and H. Krakauer, Ferroelectr. **136**, 65 (1992).

[33] A. Safari and E. K. Akdogan, *Piezoelectric and Acoustic Materials for Transducer Applications* (Springer, New York, 2008).

[34] P. Erhart, R.-A. Eichel, P. Träskelin, and K. Albe, Phys. Rev. B **76**, 174116 (2007).

[35] Z. Alahmed and H. Fu, Phys. Rev. B **76**, 224101 (2007).

[36] A. Chandrasekaran, D. Damjanovic, N. Setter, and N. Marzari, Phys. Rev. B **88**, 214116 (2013).

[37] T. Shimada, T. Ueda, J. Wang, and T. Kitamura, Phys. Rev. B **87**, 174111 (2013).

[38] R. Gerson, J. Appl. Phys. **31**, 188 (1960).

[39] R. R. Garipov, J.-M. Spaeth, and D. J. Keeble, Phys. Rev. Lett. **101**, 247604 (2008).

[40] D. J. Keeble, M. Loyo-Menoyo, Z. I. Y. Booq, R. R. Garipov, V. V. Eremkin, and V. Smotrakov, Phys. Rev. B **80**, 014101 (2009).

[41] R. A. Mackie, A. Peláiz-Barranco, and D. J. Keeble, Phys. Rev. B **82**, 024113 (2010).

[42] H. Meštrić, R.-A. Eichel, T. Kloss, K.-P. Dinse, S. Laubach, S. Laubach, P. C. Schmidt, K. A. Schönau, M. Knapp, and H. Ehrenberg, Phys. Rev. B **71**, 134109 (2005).

[43] P. Erhart and K. Albe, Comput. Mater. Sci. **103**, 224 (2015).

[44] F.-F. Ge, W.-D. Wu, L.-H. Cao, X.-M. Wang, H.-P. Wang, Y. Dai, H.-B. Wang, and J. Shen, Ferroelectrics **401**, 154 (2010).

[45] P. Erhart, P. Träskelin, and K. Albe, Phys. Rev. B **88**, 024107 (2013).

[46] R.-A. Eichel, P. Erhart, P. Träskelin, K. Albe, H. Kungl, and M. J. Hoffmann, Phys. Rev. Lett. **100**, 095504 (2008).

[47] J. Robertson, W. L. Warren, B. A. Tuttle, D. Dimos, and D. M. Smyth, Appl. Phys. Lett. **63**, 1519 (1993).

[48] J. Robertson, W. L. Warren, and B. A. Tuttle, J. Appl. Phys. **77**, 3975 (1995).

[49] R. Schafranek, S. Li, F. Chen, W. Wu, and A. Klein, Phys. Rev. B **84**, 045317 (2011).

[50] G. Geneste, B. Amadon, M. Torrent, and G. Dezanneau, Phys. Rev. B **96**, 134123 (2017).

[51] V. I. Anisimov, J. Zaanen, and O. K. Andersen, Phys. Rev. B **44**, 943 (1991).

[52] G. Kresse and J. Furthmüller, Phys. Rev. B **54**, 11169 (1996).

[53] G. Kresse and J. Furthmüller, Comput. Mater. Sci. **6**, 15 (1996).

[54] G. Kresse and D. Joubert, Phys. Rev. B **59**, 1758 (1999).

[55] P. E. Blöchl, Phys. Rev. B **50**, 17953 (1994).

[56] J. P. Perdew, K. Burke, and M. Ernzerhof, Phys. Rev. Lett. **77**, 3865 (1996).

[57] J. L. Gavartin, P. V. Sushko, and A. L. Shluger, Phys. Rev. B **67**, 035108 (2003).

[58] M. Nolan and G. W. Watson, J. Chem. Phys. **125**, 144701 (2006).

[59] B. Sadigh, P. Erhart, and D. Åberg, Phys. Rev. B **92**, 075202 (2015).

[60] J. Heyd, G. E. Scuseria, and M. Ernzerhof, J. Chem. Phys. **118**, 8207 (2003).

[61] G. Y. Gou, J. W. Bennett, H. Takenaka, and A. M. Rappe, Phys. Rev. B **83**, 205115 (2011).

[62] J. A. Rodriguez, A. Etxeberria, L. González, and A. Maiti, J. Chem. Phys. **117**, 2699 (2002).

[63] D. I. Bilc, R. Orlando, R. Shaltaf, G.-M. Rignanese, J. Íñiguez, and P. Ghosez, Phys. Rev. B **77**, 165107 (2008).

[64] M. Leslie and N. J. Gillan, J. Phys. C **18**, 973 (1985).

[65] V. G. Gavrilyachenko and E. G. Fesenko, Sov. Phys. Crystallogr. USSR **16**, 549 (1971).

[66] I. Petousis, W. Chen, G. Hautier, T. Graf, T. D. Schladt, K. A. Persson, and F. B. Prinz, Phys. Rev. B **93**, 115151 (2016).

[67] E. Cockayne and B. P. Burton, Phys. Rev. B **62**, 3735 (2000).

[68] E. Havinga, J. Phys. Chem. Solids **18**, 253 (1961).

[69] J. Hong, G. Catalan, J. F. Scott, and E. Artacho, J. Phys.: Condens. Matter **22**, 112201 (2010).

[70] M. M. Vijatović, J. D. Bobić, and B. D. Stojanović, Sci. Sintering **40**, 235 (2008).

[71] G. Henkelman and H. Jónsson, J. Chem. Phys. **113**, 9978 (2000).

[72] N. A. Deskins and M. Dupuis, Phys. Rev. B **75**, 195212 (2007).

[73] L. Sun, X. Huang, L. Wang, and A. Janotti, Phys. Rev. B **95**, 245101 (2017).

[74] P. Borlido, J. Doumont, F. Tran, M. A. L. Marques, and S. Botti, J. Chem. Theory Comput. **16**, 3620 (2020).

[75] A. Alkauskas, M. D. McCluskey, and C. G. Van de Walle, J. Appl. Phys. **119**, 181101 (2016).

[76] C. Freysoldt, B. Grabowski, T. Hickel, J. Neugebauer, G. Kresse, A. Janotti, and C. G. Van de Walle, Rev. Mod. Phys. **86**, 253 (2014).

[77] I. G. Austin and N. F. Mott, Adv. Phys. **50**, 757 (2001).

[78] F. Zhou, B. Sadigh, P. Erhart, and D. Åberg, npj Comput. Mater. **2**, 16022 (2016).

[79] Z. Wang and K. H. Bevan, Phys. Rev. B **93**, 024303 (2016).

[80] T. Hasegawa, M. Shirai, and K. Tanaka, J. Lumin. **87-89**, 1217 (2000).

[81] H. Ihrig, J. H. T. Hengst, and M. Klerk, Z. Phys. B: Condens. Matter **40**, 301 (1981).